LYMPHOID NEOPLASIA

Dosage-dependent tumor suppression by histone deacetylases 1 and 2 through regulation of c-Myc collaborating genes and p53 function

Marinus R. Heideman,[1] Roel H. Wilting,[1] Eva Yanover,[1] Arno Velds,[2] Johann de Jong,[3] Ron M. Kerkhoven,[4] Heinz Jacobs,[2] Lodewyk F. Wessels,[3] and Jan-Hermen Dannenberg[1]

[1]Division of Gene Regulation, [2]Division of Immunology, [3]Division of Molecular Carcinogenesis, [4]Genomics Core Facility, Netherlands Cancer Institute, Plesmanlaan, Amsterdam, The Netherlands

Key Points

- Hdac1 and Hdac2 are dosage-dependent tumor suppressors.
- Hdac1 and Hdac2 regulate p53-modulating genes as a barrier to prevent Myc-driven tumorigenesis.

Histone deacetylases (HDACs) are epigenetic erasers of lysine-acetyl marks. Inhibition of HDACs using small molecule inhibitors (HDACi) is a potential strategy in the treatment of various diseases and is approved for treating hematological malignancies. Harnessing the therapeutic potential of HDACi requires knowledge of HDAC-function in vivo. Here, we generated a thymocyte-specific gradient of HDAC-activity using compound conditional knockout mice for Hdac1 and Hdac2. Unexpectedly, gradual loss of HDAC-activity engendered a dosage-dependent accumulation of immature thymocytes and correlated with the incidence and latency of monoclonal lymphoblastic thymic lymphomas. Strikingly, complete ablation of Hdac1 and Hdac2 abrogated lymphomagenesis due to a block in early thymic development. Genomic, biochemical and functional analyses of pre-leukemic thymocytes and tumors revealed a critical role for Hdac1/Hdac2-governed HDAC-activity in regulating a p53-dependent barrier to constrain Myc-overexpressing thymocytes from progressing into lymphomas by regulating Myc-collaborating genes. One Myc-collaborating and p53-suppressing gene, *Jdp2*, was derepressed in an Hdac1/2-dependent manner and critical for the survival of Jdp2-overexpressing lymphoma cells. Although reduced HDAC-activity facilitates oncogenic transformation in normal cells, resulting tumor cells remain highly dependent on HDAC-activity, indicating that a critical level of Hdac1 and Hdac2 governed HDAC-activity is required for tumor maintenance. (*Blood*. 2013;121(11):2038-2050)

Introduction

Cancer develops and persists as a result of accumulating genetic and epigenetic changes.[1] The reversibility of epigenetic changes has generated increasing interest in the development of agents that target epigenetic regulators such as histone deacetylases (HDACs).[2]

HDACs are critical epigenetic erasers of lysine-acetyl marks of histones and non-histone substrates.[3] They can be classified on the basis of their homology to yeast counterparts. Class I HDACs (HDAC1, −2, −3, and −8) are highly homologous to *Saccharomyces cerevisiae Rpd3*. Class IIa HDACs (HDAC4, −5, −7, and −9) and class IIb HDACs (HDAC6 and −10) consist of *S. cerevisiae* Hda1 homologs. HDAC11 is the sole member of the class IV HDACs, based on homology to both class I and class II HDACs.[4] While class I, II, and IV HDACs are Zn^{2+}-dependent hydrolases, class III histone deacetylases, which consist of yeast *Sir2* homologs (Sirtuins 1-7), form a structurally and mechanistically distinct class of nicotinamide adenine dinucleotide dependent hydrolases.

A classic function of HDACs relates to their role as transcriptional corepressors through deacetylation of lysine residues in histone tails. This results in a closed chromatin structure and diminished accessibility for the basal transcription machinery. Class I HDACs are present in repressor complexes such as SIN3A, NuRD, REST, and *N*-CoR/SMRT, which acquire their regional activities in part by interacting with sequence-specific transcription factors.

In agreement with a high sequence similarity between class I HDAC1 and HDAC2, genetic studies in mice revealed redundant functions of these enzymes in many cell types.[5-10] In addition, many biological processes, such as DNA damage repair, autophagy, hematopoiesis, and cell cycle regulation, are collectively regulated by HDAC1 and HDAC2.[5,6,11,12]

Nevertheless, Hdac1- and Hdac2-specific functions have been identified. Deletion of Hdac1 results in embryonic lethality as early as E9.5 of development.[13] In effector T cells, Hdac1 regulates the inflammatory response in an in vivo allergic airway inflammation model, suggesting that Hdac1 has a specific function in controlling an inflammatory response by modulating cytokine expression.[14] In contrast to Hdac1 deficiency, Hdac2 loss of function results in viable mice with reduced body weight.[15-17] Others have reported that Hdac2 deficiency is not compatible with life due to cardiac myopathy.[7] In addition, Hdac2 plays a specific role in repression of genes involved in synaptogenesis, as evidenced by enhanced synapse formation, learning, and memory in Hdac2-deficient mice.[17]

The use of pharmacological HDAC inhibition in cancer treatment is rationalized by observations showing high expression of individual

Submitted August 21, 2012; accepted December 26, 2012. Prepublished online as *Blood* First Edition paper, January 17, 2013; DOI 10.1182/blood-2012-08-450916.

The online version of this article contains a data supplement.

There is an Inside *Blood* commentary on this article in this issue.

The publication costs of this article were defrayed in part by page charge payment. Therefore, and solely to indicate this fact, this article is hereby marked "advertisement" in accordance with 18 USC section 1734.

HDACs and recruitment of these proteins by oncogenic fusion proteins such as PML-RAR and AML-ETO in various cancer types.[18] In contrast, class I HDACs, such as HDAC1 and HDAC2, have been identified in complexes harboring tumor suppressors, such as the retinoblastoma protein (RB1),[19] p53,[20] BCL11B,[21] and RUNX1.[22] Hence, inhibition of HDACs may have tumor-promoting and tumor-suppressive consequences. The growing interest in the use of HDACi and other epigenetic drugs as therapeutic agents in the treatment of cancer, acquired drug resistance, HIV, diabetes, and neurological disorders such as Alzheimer disease[23-26] necessitate full knowledge of HDACs in normal development to harness the therapeutic potential and future development of novel HDACi.

Methods

Mice

The *Hdac1* and *Hdac2* cKO alleles as well as *MxCre;Hdac1$^{L/L}$;Hdac2$^{L/L}$* mice have been described elsewhere.[5,17] Thymocyte-specific deletion of Hdac1 and Hdac2 was obtained using *LckCre* transgenic mice[27] in combination with *Hdac1* and/or *Hdac2* cKO alleles. All cohorts were in a mixed FVB/n, C57BL/6, and 129/Sv background. All experiments were approved by a local ethical committee and performed according to national guidelines.

Establishment, culturing, and treatment of mouse thymic lymphoma tumor cell lines

Tumors were dissected from the thorax of *LckCre;Hdac1$^{\Delta/\Delta}$*, *LckCre;Hdac1$^{+/\Delta}$*; *Hdac2$^{\Delta/\Delta}$*, *LckCre;Hdac1$^{\Delta/\Delta}$;Hdac2$^{+/\Delta}$*, *Eμ-Myc, or p53$^{-/-}$* mice. Single cell suspensions were cultured in Dulbecco's modified Eagle medium or Iscove modified Dulbecco medium medium containing 10% fetal bovine serum, glutamine, penicillin/streptomycin supplemented with 20% Methocult (M3434, Stem Cell Technologies). CD4 and CD8 flow cytometry analysis was used to confirm the T-cell identity of the cell lines. To determine HDACi sensitivity, tumor cell lines were treated with different concentrations of suberoylanilide hydroxamic acid (SAHA; Selleck) for 72 hours. Cell viability was measured using Cell Titer Blue assay (Promega). To infect lymphoma cell lines with lentiviral shRNA constructs, 5×10^5 cells were infected twice with 30 μL of concentrated lentiviral supernatants containing 4 μg/mL polybrene in a total volume of 530 μL for 24 hours and subsequently selected with 2.0 μg/mL puromycin for at least 48 hours. pLKO.1 *Jdp2* and nontargeting (NT) shRNA vectors were obtained from the Netherlands Cancer Institute Robotics and Screening facility. *Jdp2* mRNA levels were analyzed by quantitative polymerase chain reaction (qPCR) using the following primers: *Jdp2*_F 5′-CGCTGACATCCGCAACATTG-3′, *Jdp2*_R 5′-CATCTGGCTG CAGCGACTTT-3′.

In vivo BrdU labeling

Mice were injected intraperitoneally with 200 μL 5-bromo-2'-deoxyuridine (BrdU) solution (10 mg/mL). After 1.5 hours, thymocytes were intracellularly labeled with Bride antibodies (α-BrdU-APC) and with the DNA binding fluorescent dye 7-AAD (BrdU Flow Kit, BD Pharmingen). Subsequently, stained thymocytes were analyzed on a multicolor CyAn flow-cytometer (Beckman Coulter). Data were analyzed with FlowJo software (Treestar).

Histology

Tissues were fixed in ethanol–acetic acid–formol saline for 24 hours and subsequently embedded in paraffin. For immunohistochemistry, sections were preincubated with goat serum (Sanquin) for 30 minutes and subsequently incubated o/n with an Hdac1 antibody (Abcam), Hdac2 (Invitrogen), or p53 (VectorLabs) and secondary poly-HRP-anti-rabbit IgG (Immunologic) for 30 minutes. The slides were washed with phosphate-buffered saline, incubated with 3′3-diamino benzidine substrate chromogen system (Dako), and counterstained with hematoxylin (Merck).

Flow cytometry

Thymocytes and thymic lymphoma cells were stained with Thy1-PE, CD4-PacificBlue, CD8-FITC (fluorescein isothiocyanate), CD25-PerCP-Cy5.5, CD44-APC, TCRβ-APC, and CD24-PE (BD Biosciences). Apoptotic thymocytes were determined using an antibody against annexinV (annexinV apoptosis kit, BD Biosciences) and propidium iodide (PI) counterstain. All experiments were performed using a multicolor CyAn flow cytometer (Beckman Coulter). Data were analyzed with FlowJo software (Treestar).

Western blot analysis

For western blot analysis, tissues and cells were lysed in radioimmunoprecipitation assay buffer (20 mM Tris, pH7.5, 150 mM sodium chloride, 1% Nonidet P-40, 0.5% sodium deoxycholate, 1 mM EDTA, 0.1% sodium dodecyl sulfate), protease inhibitors (Roche), phosphatase inhibitors, 5 μM trichostatin A, and 1 mM nicotinamide. We used 20 μg of total protein for western blotting and incubated it with antibodies against Hdac1 (IMG-337, Imgenex), Hdac2 (SC-7899, Santa Cruz), Hdac3 (Cell Signaling), Hdac8 (Santa Cruz), and γ-tubulin (T6557, Sigma). Protein levels were quantified using IRDye 680/800CW secondary antibodies (Li-Cor). Nitrocellulose membranes were stained and imaged with the LI-COR Odyssey infrared imaging system. Other antibodies used are against p19^{Arf} (Ab80; Abcam), p53 (IMX25, Novocastra), c-Myc (*N*-262, Santa Cruz), green fluorescent protein (GFP) (11814460001, Roche) acetylated H3 (06599, Millipore), acetylated H4 (06866, Millipore), histone H3 (Ab1791, Abcam), histone H4, and horseradish peroxidase coupled secondary antibodies (Dako). Western blots were stained with enhanced chemiluminescence (Pierce), imaged, and quantified with ChemiDoc software (BioRad).

Southern blot analysis

Genomic DNA (10 μg) of tumor samples or primary thymocytes was digested with *EcoR*I overnight at 37°C. The DNA fragments were separated on a 0.8% agarose gel and transferred to a nitrocellulose membrane. The blots were hybridized with a ^{32}P-labeled probe harboring the *Jβ2* region of the *TCRβ* locus.

HDAC activity assay

Lysates from fresh thymocytes were assayed for HDAC activity using the HDAC fluorimetric activity assay kit (Enzo life Sciences)

Comparative genomic hybridization

Genomic DNA was isolated from tumor samples using the Puregene purification kit (Qiagen). As a reference, we used genomic tail DNA from the same mouse. Tumor and tail DNA were Cy3 and Cy5 labeled using the Dual Color labeling kit (Nimblegen) according to the manufacturer's instructions. Labeled DNAs were hybridized onto mouse comparative genome hybridization (CGH) 12 × 135K whole-genome tiling arrays. The arrays were scanned on an Agilent scanner (model G2505B) at a resolution of 2 μm double pass at 100% gain of photo multiplier tubes for both channels. The data were analyzed with NimbleScan software (Nimblegen). aCGH data were deposited at the GEO database: accession number GSE43407

Chromosome spreads

Cells were incubated for 90 minutes in medium with 0.05 μg/mL colcemid (Gibco). Hereafter, the cells were washed with phosphate-buffered saline and resuspended in 75 mM potassium chloride and incubated at 37°C for 10 minutes. Subsequently the cells were fixed in methanol/acetic acid (3:1) and dropped on microscope slides. These slides were dried and cells were mounted with Vectashield/DAPI (Vector Laboratories).

Methylation genomic DNA tumors

Genomic DNA was isolated and digested with methylation-sensitive (*Hpa*II) or -insensitive restriction enzymes (*Msp*I) and analyzed on DNA Southern blots. As a probe for methylation analysis of minor satellites, we used pMR150.

Transcriptome analysis and bioinformatics

For gene expression analysis, total RNA from thymi or tumor tissue was extracted, labeled, and hybridized onto Illumina MouseWG-6 v2.0 Expression BeadChip Arrays by the Netherlands Cancer Institute Central Microarray and Deep Sequencing Core Facility according to the manufacturer's protocol. We mapped 20 312 MuLV integration sites from 1020 tumors in mice with various genetic backgrounds[28] to their putative target genes using a kernel-convolved rule-based mapping approach (KC-RBM)[29] and the Ensembl reference genome (build 61). Commonly targeted genes (CTGs) were called based on a threshold of at least 1 insertion per target gene. A set of 547 genes consistently deregulated in $Hdac1^{\Delta/\Delta}$;$Hdac2^{\Delta/+}$ thymocytes and lymphomas were mapped to mouse Ensembl gene identifiers. Overlap between the resulting 413 mouse Ensembl identifiers and the CTGs was then assessed by performing a Fisher exact test, using the complete set of Ensembl gene identifiers as a reference. Gene expression data were deposited at the ArrayExpress database: accession number E-MTAB-1448

Tissue Microarray

A tissue microarray (TMA) was generated by collecting 3 cores of tumor or normal tissue, as determined by hematoxylin-eosin–stained paraffin-embedded lymphomas as well as 3-week-old thymi. For control and orientation purposes, cores of paraffin-embedded wild-type liver were included in the TMA. Cores were embedded in a paraffin block and subsequently sectioned in 3-μm slides. Hdac1, Hdac2, and p53 staining were performed as described above. Hdac1 staining and Hdac2 staining were used to confirm the genotype of the lymphoma. Scoring for p53 staining intensity was performed by using a p53-mutant lymphoma as a positive control and wild-type thymus as a negative control. A score was assigned only when all 3 cores showed a consistent staining pattern.

p53 status assessment by sequencing, γ-irradiation, and Nutlin-3 treatment

To determine *p53* sequence, genomic DNA of primary thymocytes and tumor cell lines was isolated with a DNeasy Blood & Tissue kit (Qiagen). *p53* exon 2-11 were PCR amplified and sequenced on a 3730 DNA analyzer (Applied Biosystems). To determine DNA damage–mediated p53 induction, thymocytes were irradiated with 6 Gy using the Gammacell 40 EXACTOR and tumor cell lines were treated with 8 μM Nutlin-3 (Cayman Chemical). Irradiated thymocytes were cultured for 16 hours and treated with Nutlin-3 for 6 hours and subsequently analyzed for p53 protein expression. For the apoptosis assay, 2×10^6 fresh thymocytes were irradiated with 0, 2, 4, 6, 8, and 10 Gy and cultured for 16 hours. Apoptosis was assayed by staining with annexinV and PI and performing subsequent analysis by flow cytometry (FITC-annexinV apoptosis kit, BD-Biosciences).

Chromatin immunoprecipitation

Chromatin immunoprecipitation was performed by cross-linking chromatin from 5×10^7 $p53^{-/-}$ T-cell lymphoma cells expressing GFP, Hdac1-GFP, or Hdac2-GFP (R.H.W and J.-H.D, unpublished results) using 1% formaldehyde for 10 minutes at room temperature. Cross-linking was stopped in 1.25 M glycine for 5 minutes on ice. Chromatin was subsequently sonicated in lysis buffer (50 mM Tris-HCl pH 8.0, 10 mM EDTA, 1% SDS, protease inhibitors [Roche]) using a probe sonicator (Bandelin, cycle 90%, output 8, 15 seconds on/off) and subsequently diluted in dilution buffer (10 mM Tris-HCl pH 8.0, 160 mM NaCl, 5 mM EDTA, 1% Triton X-100, protease inhibitors). Chromatin was incubated overnight with 10 μL of 10% bovine serum albumin–blocked GFP-Trap beads (ChromoTek) in dilution buffer at 4°C. Chromatin-bound beads were washed with radioimmunoprecipitation assay buffer (50 mM Tris-HCl pH 8.0, 150 mM NaCl, 0.1% SDS, 0.5% NaDOC, 1% NP-40, protease inhibitors) and with Tris-EDTA (10 mM Tris-HCl, pH 8.0, 1 mM EDTA). To elute chromatin, the beads were incubated in Tris-EDTA plus 2% SDS at 65°C for 15 minutes while shaking. Cross-links were reverted by incubating chromatin at 68°C overnight with proteinase K. DNA was purified using MinElute PCR purification columns (Qiagen) and subjected to quantitative PCR using the Roche LightCycler system. Primers used for qPCR are *Jdp2* 5′ UTR: 5′-TGTGAGCTGTCACCCATCAT-3′, 5′-CCA CCCCAGATAGAGAAGCA-3′; *Jdp2* intron 1-2: 5′-ATGCTATGGC TCTGCGTTCT-3′, 5′-TGACCCCTCAAGACAACCTC-3′.

Results

Spontaneous lymphomagenesis in $MxCre^+$;$Hdac1^{L/L}$ and $MxCre^+$;$Hdac1^{L/L}$;$Hdac2^{L/L}$ mice

To study HDAC function in vivo, we previously generated conditional knockout alleles for Hdac1[5] and Hdac2.[17] While interferon-inducible *Mx*Cre-recombinase–mediated deletion of *Hdac1* and *Hdac2* in the hematopoietic system resulted in anemia and thrombocytopenia-related death,[5] we noted that aging, uninduced, $MxCre^+$;$Hdac1^{L/L}$ and $MxCre^+$;$Hdac1^{L/L}$;$Hdac2^{L/L}$ mice became lethargic and presented in all cases $CD4^+CD8^+$ thymic lymphomas (Figure 1A,B [top panel]). Intriguingly, $MxCre^+$;$Hdac1^{L/L}$;$Hdac2^{L/L}$ mice developed tumors with a higher incidence (85% vs 25%) and shorter latency (15 weeks vs 25 weeks) compared with $MxCre^+$;$Hdac1^{L/L}$ mice. While Hdac1 expression was absent in lymphomas derived from $MxCre^+$;$Hdac1^{L/L}$ and $MxCre^+$;$Hdac1^{L/L}$;$Hdac2^{L/L}$ mice, lymphomas derived from both genotypes still expressed Hdac2 (Figure 1B [bottom panel] and supplemental Figure 1A). Interestingly, genetic analysis of $MxCre^+$;$Hdac1^{L/L}$;$Hdac2^{L/L}$ lymphoma cell lines derived from primary tumors exclusively displayed complete loss of *Hdac1*, whereas only 1 conditional *Hdac2* allele was deleted (supplemental Figure 1B). These results indicate that leaky Cre expression from the *Mx* promoter resulted in sporadic deletion of *Hdac1* and *Hdac2*. Apparently, loss of Hdac1 or mono-allelic expression of Hdac2 in the absence of Hdac1 conferred a selective advantage in thymocytes, resulting in lymphomagenesis, which uncovers a previously unknown tumor suppressor function for Hdac1 and Hdac2. In addition, the differential lymphoma incidence in $MxCre^+$;$Hdac1^{L/L}$ and $MxCre^+$;$Hdac1^{L/L}$;$Hdac2^{L/L}$ mice suggests a dosage dependency in tumor suppression by Hdac1 and Hdac2.

Thymocyte-specific deletion of Hdac1 and Hdac2 results in an HDAC activity gradient

To test whether Hdac1 and Hdac2 suppress tumorigenesis in a dosage-dependent manner, we generated a thymocyte-specific series of inactivated *Hdac1* and *Hdac2* alleles using *Lck*-promoter–driven Cre-recombinase expression. Western blot analysis of isolated thymocytes from these mice indicated efficient deletion of Hdac1 and Hdac2 (supplemental Figure 2A,B). Ablation of Hdac1 resulted in elevated Hdac2 protein levels, while class I Hdac3 and Hdac8 proteins levels were unaffected (supplemental Figure 2B). While Hdac2 deficiency did not result in increased Hdac1 proteins levels, loss of 1 allele of Hdac1 in the absence of Hdac2 resulted in elevated Hdac1 protein levels. These results suggest compensatory regulation of Hdac1 and Hdac2 protein levels in thymocytes (supplemental Figure 2B).

Deletion of combinations of *Hdac1* and *Hdac2* alleles resulted in differential effects on global HDAC activity, as HDAC-activity measurements in 1-week-old thymocytes revealed a progressive loss of global HDAC activity in wild-type $>$ $Hdac1^{+/\Delta}$;$Hdac2^{\Delta/\Delta}$ $\geq$ $Hdac1^{\Delta/\Delta}$ $>$ $Hdac1^{\Delta/\Delta}$;$Hdac2^{+/\Delta}$ thymocytes (Figure 1C). Although ablation of Hdac1 resulted specifically in elevated Hdac2 protein levels in $Hdac1^{\Delta/\Delta}$ thymocytes (supplemental Figure 2B), it could only partially compensate for the loss of global HDAC activity (Figure 1C). Indeed, mono-allelic expression of Hdac2 in Hdac1-

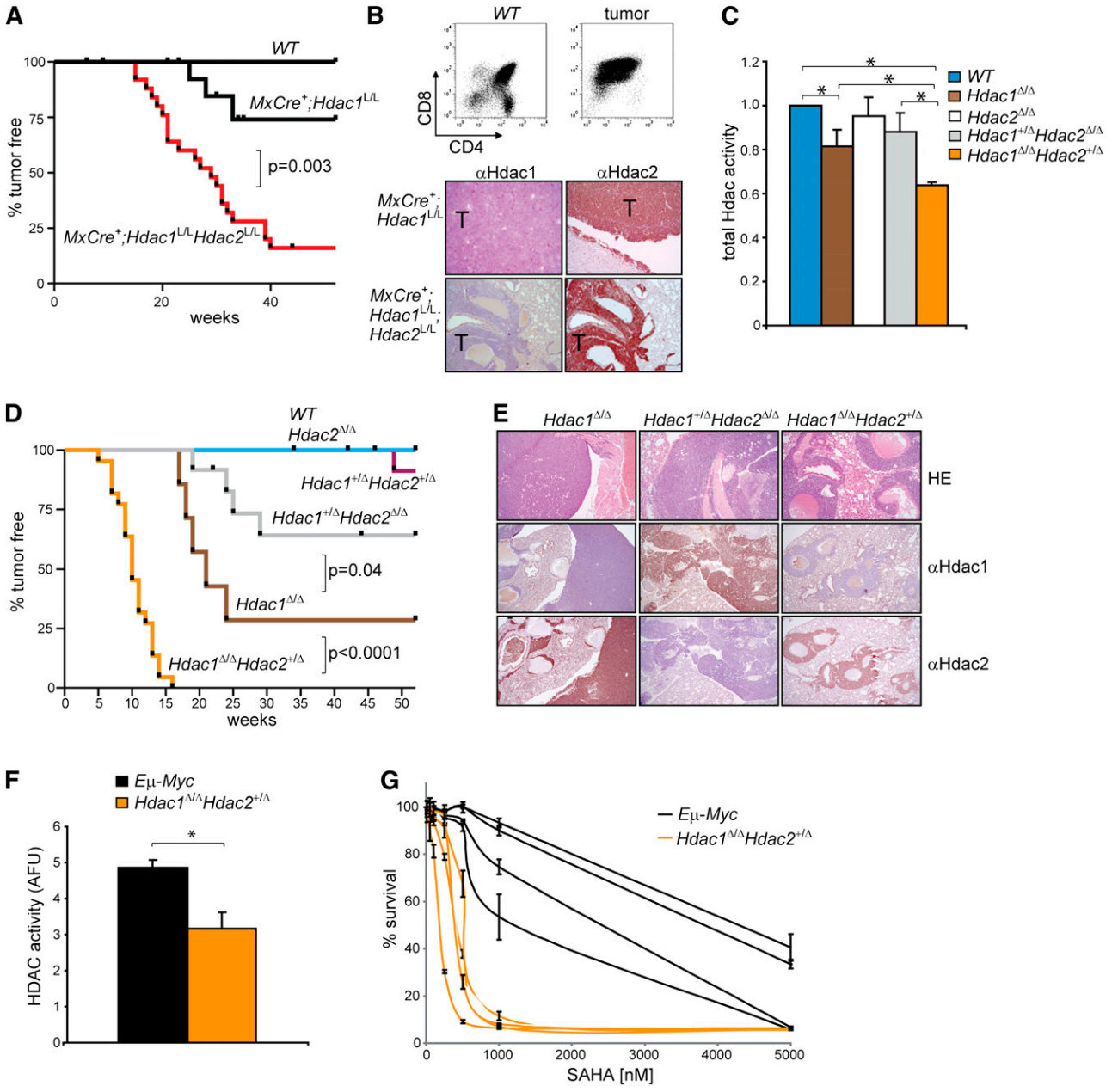

Figure 1. Hdac1 and Hdac2 dosage-dependent tumor suppression. (A) Kaplan-Meier tumor-free survival plot of *WT*, *MxCre*$^{+}$;*Hdac1*$^{L/L}$ and *MxCre*$^{+}$;*Hdac1*$^{L/L}$*Hdac2*$^{L/L}$ mice. *P* value was calculated using a χ^2 test. (B) CD4/CD8 flow cytometry (top) and Hdac1 and Hdac2 immunohistochemistry (bottom) of tumors from *MxCre*$^{+}$;*Hdac1*$^{L/L}$ and *MxCre*$^{+}$;*Hdac1*$^{L/L}$*Hdac2*$^{L/L}$ mice. (C) Global HDAC activity in thymocytes with indicated genotypes relative to *WT* thymocytes. (D) Kaplan-Meier tumor-free survival plot of mice harboring thymocytes with indicated genotypes. *P* values were calculated using a χ^2 test. (E) Representative pictures of Hdac1 and Hdac2 immunohistochemical analysis of lymphomas with indicated genotypes. Magnification: 100×. (F) Global HDAC activity in 4 independent *Eμ−Myc* and 4 independent *Hdac1*$^{\Delta/\Delta}$;*Hdac2*$^{\Delta/+}$ tumor cell lines. (G) Dose response curves of 4 independent *Eμ−Myc* and 4 independent *Hdac1*$^{\Delta/\Delta}$;*Hdac2*$^{\Delta/+}$ tumor cell lines treated increasing concentrations of suberoylanilide hydroxamic acid (SAHA). Error bars indicate standard deviations of 3 independent experiments per tumor cell line. *WT*, wild type.

deficient (*Hdac1*$^{\Delta/\Delta}$;*Hdac2*$^{+/\Delta}$) thymocytes resulted in a further reduction of HDAC activity (Figure 1C). These results indicate a dynamic interplay between Hdac1 and Hdac2 in contributing to global HDAC activity in thymocytes in which Hdac1 seems to act as dominant histone deacetylase. In conclusion, we established an in vivo gradient of Hdac1 and Hdac2 activity that provides a unique model to study HDAC-activity dosage in tumor suppression.

Hdac1 and Hdac2 dosage-dependent tumor suppression

To test whether stepwise reduction of HDAC activity resulted in tumorigenesis, we monitored cohorts of mice carrying combinations of inactivated *Hdac1* and *Hdac2* alleles over time. Intriguingly, a progressive reduction of HDA activity correlated with increased tumorigenesis in mice. Whereas *LckCre;Hdac1*$^{+/\Delta}$;*Hdac2*$^{\Delta/\Delta}$ mice developed tumors with a 25% incidence and a mean latency of >52 weeks, tumor incidence increased significantly in *LckCre;Hdac1*$^{\Delta/\Delta}$ mice with a 75% incidence and a 23-week mean latency. Consistent with a further reduction of global HDAC activity, tumorigenesis was drastically accelerated in *LckCre;Hdac1*$^{\Delta/\Delta}$;*Hdac2*$^{+/\Delta}$ mice, with a 100% tumor incidence and a mean latency of 10 weeks (Figure 1D). Tumors across genotypes were identified as thymic lymphomas, which disseminated predominantly to lung, kidney, liver, and lymph nodes (supplemental Figure 2C,D). Mono-allelic expression of Hdac1

and Hdac2 was maintained in *Hdac1*$^{+/\Delta}$;*Hdac2*$^{\Delta/\Delta}$ and *Hdac1*$^{\Delta/\Delta}$;*Hdac2*$^{+/\Delta}$ lymphomas, as evidenced by Hdac1 and Hdac2 immunohistochemical staining on paraffin-embedded primary tumors and genomic analysis of *Hdac1* and *Hdac2* alleles in lymphoma cell lines (Figure 1E; supplemental Figure 2E). These findings were corroborated by the appearance of a thymic lymphoma in 1 of 10 *LckCre;Hdac1*$^{+/\Delta}$;*Hdac2*$^{+/\Delta}$ mice at 46 weeks that lost Hdac1 and retained Hdac2 expression (Figure 1D and supplemental Figure 2F). Genetic analysis of this tumor indicated loss of the wild-type *Hdac1* allele and maintenance of 1 wild-type *Hdac2* copy, thereby recapitulating *Hdac1*$^{\Delta/\Delta}$;*Hdac2*$^{+/\Delta}$ tumors (supplemental Figure 2G). This result suggests that reduced Hdac1 and Hdac2 levels generate a tumor-prone condition that allows in vivo selection for *Hdac1* loss of heterozygosity.

In summary, we established, for the first time, a tumor suppressor function for Hdac1 and Hdac2, which act collectively in a dosage-dependent manner.

Complete loss of Hdac1 and Hdac2 abrogates lymphomagenesis

Surprisingly, further reduction of Hdac1 and Hdac2 in *LckCre;Hdac1*$^{\Delta/\Delta}$;*Hdac2*$^{\Delta/\Delta}$ (*DKO*) mice never resulted in tumors lacking both Hdac1 and Hdac2. However, it did result in selection for *Hdac1*$^{\Delta/\Delta}$;*Hdac2*$^{\Delta/+}$ thymocytes and consequently *Hdac1*$^{\Delta/\Delta}$;*Hdac2*$^{\Delta/+}$ lymphomas, thereby phenocopying *LckCre;Hdac1*$^{\Delta/\Delta}$;*Hdac2*$^{\Delta/+}$ mice. In agreement with a selection for *Hdac1*$^{\Delta/\Delta}$;*Hdac2*$^{\Delta/+}$ thymocytes in *DKO* mice, the kinetics of tumor development in *DKO* mice are significantly slower compared with that in *LckCre;Hdac1*$^{\Delta/\Delta}$;*Hdac2*$^{\Delta/+}$ mice (supplemental Figure 2H). In summary, although Hdac1 and Hdac2 suppress lymphomagenesis in a dosage-dependent manner, complete inactivation of Hdac1 and Hdac2 abrogates lymphomagenesis.

A critical level of HDAC activity is required for tumor maintenance

A complete inactivation of Hdac1 and Hdac2 abrogated lymphomagenesis suggests a requirement for critical HDAC activity to initiate or maintain tumorigenesis. Indeed, pharmacological inhibition of remaining HDAC activity in established *Hdac1*$^{\Delta/\Delta}$;*Hdac2*$^{\Delta/+}$ lymphoma cell lines resulted in a dose-dependent cell death, indicating that tumor maintenance is dependent on critical HDAC activity levels (Figure 1G). Interestingly, *Hdac1*$^{\Delta/\Delta}$;*Hdac2*$^{+/\Delta}$ lymphoma cell lines, which displayed relatively low HDAC activity compared with Hdac1/2-expressing *Eμ−Myc* lymphoma cell lines, were 2- to 10-fold more sensitive to HDACi compared with *Eμ−Myc* lymphoma cell lines (Figure 1F,G). These data show that although reduced HDAC activity facilitates oncogenic transformation in normal cells, the resulting tumor cells remain highly dependent on HDAC activity, thereby exposing a cancer cell vulnerability.

HDAC-activity, dosage-dependent increase of ISP thymocytes in preleukemic thymi

To investigate whether deregulated thymocyte development underlies lymphoma development, we analyzed T-cell differentiation in wild-type *LckCre;Hdac2*$^{\Delta/\Delta}$ *LckCre;Hdac1*$^{+/\Delta}$;*Hdac2*$^{\Delta/\Delta}$, *LckCre;Hdac1*$^{\Delta/\Delta}$, and *LckCre;Hdac1*$^{\Delta/\Delta}$;*Hdac2*$^{+/\Delta}$ mice. T-cell receptor β (*Tcrβ*) diversity analysis of *LckCre;Hdac1*$^{\Delta/\Delta}$;*Hdac2*$^{+/\Delta}$ thymi revealed a polyclonal population of thymocytes, indicative for preleukemic *Hdac1*$^{\Delta/\Delta}$;*Hdac2*$^{+/\Delta}$ thymocytes (Figure 2A). *LckCre;Hdac1*$^{\Delta/\Delta}$ and *LckCre;Hdac1*$^{\Delta/\Delta}$;*Hdac2*$^{+/\Delta}$ mice showed reduced thymocyte numbers that were associated with increased apoptosis and a specific decrease in CD4;CD8 double positive (DP) thymocytes (Figure 2B,C,D [top panel], E [left panel]). Remarkably, *LckCre;Hdac1*$^{\Delta/\Delta}$;*Hdac2*$^{+/\Delta}$ mice displayed a dramatic increase in CD8 single-positive (CD8 SP) thymocytes, which predominantly consisted of immature CD8 SP (ISP) thymocytes, as determined by CD24 and TCRβ surface markers (Figure 2D,E). Moreover, we observed a dosage-dependent expansion of the ISP thymocyte population in all lymphoma-prone genotypes (*LckCre;Hdac1*$^{+/\Delta}$;*Hdac2*$^{\Delta/\Delta}$, *LckCre;Hdac1*$^{\Delta/\Delta}$ and *LckCre;Hdac1*$^{\Delta/\Delta}$;*Hdac2*$^{+/\Delta}$) that correlated with global HDAC activity levels and tumor incidence (Figure 2D [bottom panel], E [right panel]). In vivo BrdU labeling revealed a twofold increase in the percentage of BrdU-positive cells in 1-week-old *LckCre;Hdac1*$^{\Delta/\Delta}$;*Hdac2*$^{+/\Delta}$ thymi, which consisted primarily of CD8 SP cells (Figure 2F), indicating the proliferative capacity of the expanded ISP population. These data indicate a crucial role for Hdac1 and Hdac2 in the regulation of pre–T-cell development by controlling ISP thymocytes, a T-cell developmental stage that was previously implicated in lymphomagenesis.[30] The correlations between global HDAC activity, tumor latency, and tumor incidence and ISP thymocyte numbers strongly suggests that Hdac1 and Hdac2 suppress lymphomagenesis by controlling ISP thymocytes in a dosage-dependent manner.

Hdac1 and Hdac2 are required for early thymocyte development

In order to provide a rationale for the absence of Hdac1- and Hdac2-deficient tumors in *LckCre;Hdac1*$^{\Delta/\Delta}$;*Hdac2*$^{\Delta/\Delta}$ mice, we analyzed thymi when these mice were 1 week of age. Total thymocyte numbers were dramatically reduced compared with wild-type thymocytes and *LckCre;Hdac1*$^{\Delta/\Delta}$;*Hdac2*$^{+/\Delta}$ thymocytes (Figures 3A and 2A) and associated with increased apoptosis (Figure 3B). Surprisingly, flow cytometric analysis showed a fivefold increase in CD4;CD8 double negative (DN) thymocytes specifically in *LckCre;Hdac1*$^{\Delta/\Delta}$;*Hdac2*$^{\Delta/\Delta}$ thymi, which was accompanied by a severe reduction in CD4;CD8 DP thymocytes (Figure 3C,D). Thymic analysis across genotypes revealed specifically in *DKO* thymi an early developmental block at the CD4$^-$CD8$^-$ double negative stage 3 (DN3; Figure 3D and supplemental Figure 3A,B), demonstrating that complete ablation of Hdac1 and Hdac2 is not compatible with developmental progression of early thymocytes and consequently prevents tumorigenesis. Collectively, our results show that a gradual decrease in Hdac1- and Hdac2-governed HDAC-activity predisposes to tumorigenesis, whereas complete loss of Hdac1 and Hdac2 prevents oncogenic transformation.

Chromosome 15 trisomy is associated with c-Myc overexpression in monoclonal T-cell lymphomas

Analysis of *Tcrβ* diversity revealed a monoclonal origin of *Hdac1*$^{\Delta/\Delta}$;*Hdac2*$^{+/\Delta}$ lymphomas, suggesting a requirement for additional genetic events driving full oncogenic transformation upon reduced HDAC activity (Figure 4A). CGH of normal vs tumor DNA identified, independent of genotype and HDAC activity, trisomy of chromosome 15 as a common and early genetic alteration in all analyzed lymphomas (Figure 4B). Chromosome 15 trisomy was previously observed in murine thymic lymphomas and invariably associated with overexpression of the *c-Myc* oncogene, a major driver of lymphomagenesis located on chromosome 15.[31] Indeed, c-Myc expression levels were increased in *Hdac1*$^{\Delta/\Delta}$, *Hdac1*$^{+/\Delta}$;*Hdac2*$^{\Delta/\Delta}$ and *Hdac1*$^{\Delta/\Delta}$;*Hdac2*$^{+/\Delta}$ tumors (Figure 4C,D), suggesting that during

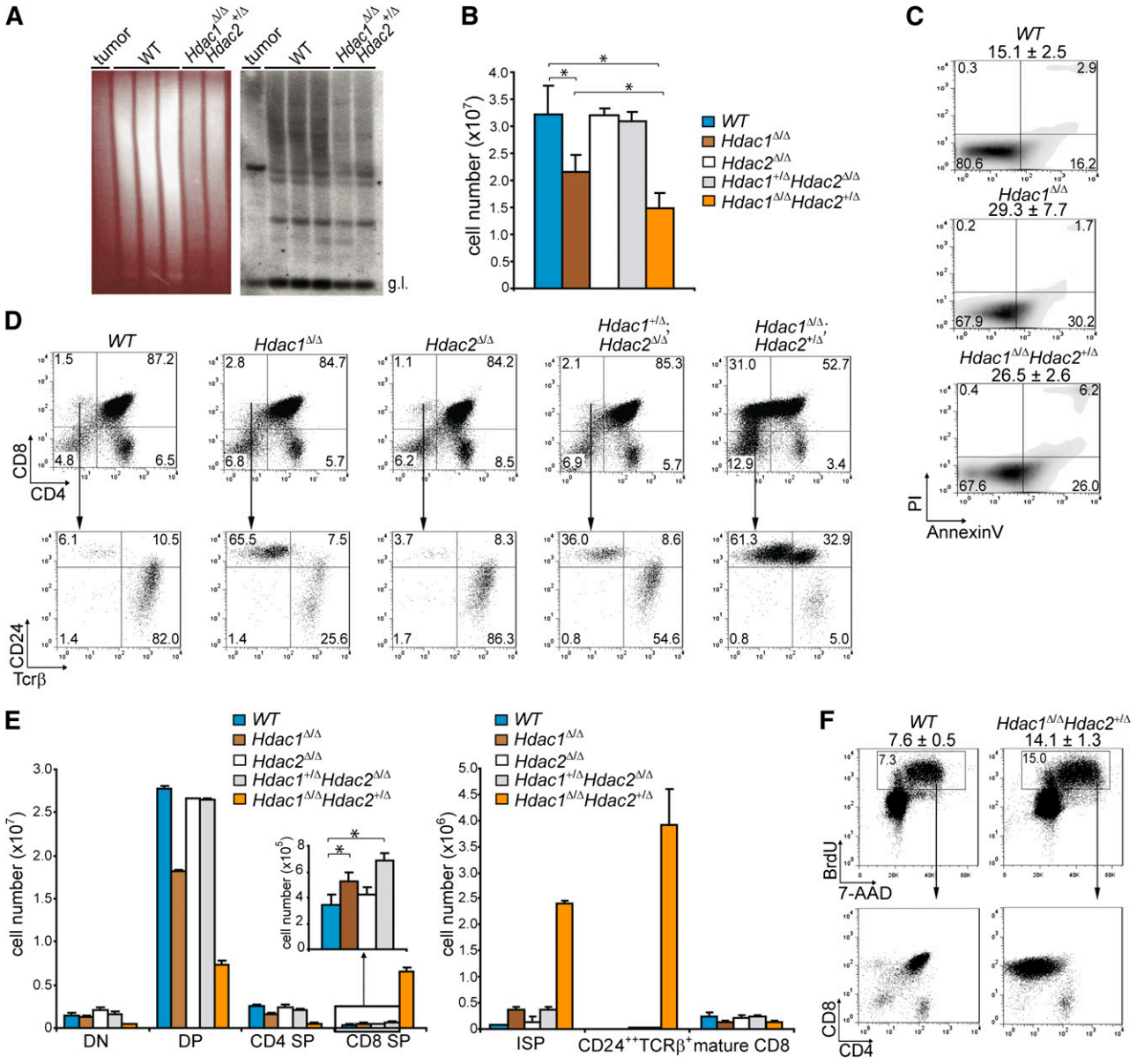

Figure 2. Hdac1 and Hdac2 control pre–T-cell development in a dosage-dependent manner. (A) *Tcrβ* repertoire determined in 3-week-old *WT* and *Hdac1*$^{\Delta/\Delta}$;*Hdac2*$^{\Delta/+}$ thymi by Southern blot analysis using a *Jβ2* probe sequence (right panel). *Hdac1*$^{\Delta/\Delta}$;*Hdac2*$^{\Delta/+}$ lymphoma DNA was used as a positive control, while ethidium bromide–stained gel served as a loading control (left panel). (B) Quantification of thymocytes from 1-week-old mice of the indicated genotypes (n = 3 per genotype). (C) Apoptosis in thymocytes of 1-week-old *WT*, *LckCre*;*Hdac1*$^{\Delta/\Delta}$ and *LckCre*;*Hdac1*$^{\Delta/\Delta}$;*Hdac2*$^{\Delta/+}$ mice, as determined by annexinV and PI staining. Mean percentages of apoptotic (annexinV$^+$PI$^-$) cells are presented on top (n = 3 mice per genotype). (D) Representative dot plots of CD4/CD8 (top) and CD24/TCRβ (bottom) flow cytometric analyses of thymi from 1-week-old mice with indicated genotypes. (E) Quantification of thymic subsets of 1-week-old mice with indicated genotypes. DN = CD4$^-$CD8$^-$, DP = CD4$^+$CD8$^+$, CD4 SP = CD4$^+$CD8$^-$, CD8 SP = CD4$^-$CD8$^+$ (left); ISP = CD4$^-$CD8$^+$CD24$^+$Tcrβ$^{+/-}$, mature CD8 = CD4$^-$CD8$^+$CD24$^{+/-}$Tcrβ$^+$ (right). (F) Dot plots representing BrdU-7-AAD flow cytometric analysis of thymocytes from *WT* and *LckCre*;*Hdac1*$^{\Delta/\Delta}$;*Hdac2*$^{\Delta/+}$ mice 1.5 hours after BrdU injection. Average and standard deviation of BrdU-positive thymocytes are indicated on top (n = 3 mice per group). *WT*, wild type.

lymphomagenesis, reduced HDAC activity allows the clonal outgrowth of c-Myc overexpressing thymocytes.

Cytogenetic analysis of *Hdac1*$^{\Delta/\Delta}$, *Hdac1*$^{+/\Delta}$;*Hdac2*$^{\Delta/\Delta}$ and *Hdac1*$^{\Delta/\Delta}$;*Hdac2*$^{+/\Delta}$ lymphoma cell lines displayed mild aneuploidy and increased centromeric attachment of multiple chromosomes (supplemental Figure 4A,B), suggesting that reduced HDAC activity may result in chromosome missegregation and generate chromosomal instability. However, analysis of preleukemic thymocytes from 1-week-old *Hdac1*$^{\Delta/\Delta}$;*Hdac2*$^{+/\Delta}$ mice revealed no chromosomal abnormalities nor altered DNA methylation of pericentric minor satellite sequences (supplemental Figure 4C,D), indicating that gradual loss of HDAC activity does not drive tumorigenesis by inducing massive, acute chromosomal instability.

Hdac1/2 dosage-dependent alleviation of p53 inactivation in lymphomagenesis

Myc-driven tumorigenesis requires inactivation of the p19^{Arf}-Mdm2-p53 pathway through either activating *Notch1* mutations, *Mdm2* amplification, inactivating *p53* mutations or deletion of the *Cdkn2a* locus encoding p16^{Ink4a} and p19^{Arf33}. *Hdac1*$^{\Delta/\Delta}$;*Hdac2*$^{+/\Delta}$ lymphomas did not harbor *Notch1* PEST domain mutations, and no

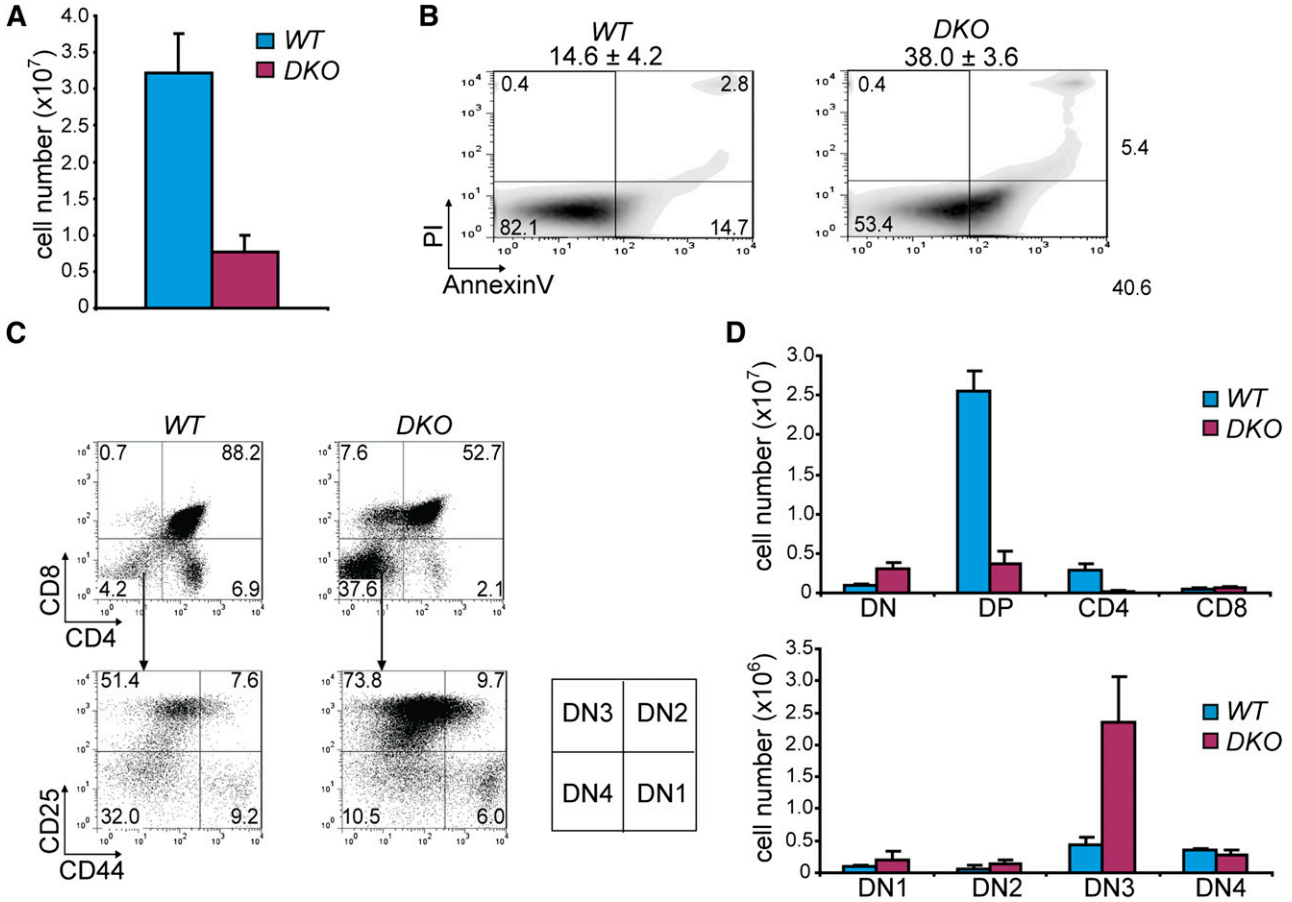

Figure 3. Hdac1 and Hdac2 collectively show obligate haploinsufficiency in tumor suppression. (A) Quantification of thymocytes in 1-week-old *WT* and *LckCre*; $Hdac1^{\Delta/\Delta}$;$Hdac2^{\Delta/\Delta}$ (*DKO*) mice (n = 3 mice per genotype). (B) Apoptosis in thymi of 1-week-old *WT* and *DKO* mice, as determined by annexinV and PI staining. Mean percentages and standard deviations of apoptotic (annexinV$^+$PI$^-$) cells are presented on top (n = 3 mice per genotype). (C) Representative CD4/CD8 (top panel) and CD25/CD44 (bottom) flow cytometry dot plots of thymocytes from 1-week-old *WT* and *DKO* mice. Scheme on the right indicates DN stages of thymocyte development. (D) Quantification of thymic subsets in 1-week-old *WT* and *DKO* mice. DN = CD4$^-$CD8$^-$; DP = CD4$^+$CD8$^+$; CD4 SP = CD4$^+$CD8$^-$; CD8 SP = CD4$^-$CD8$^+$; DN1 = CD25$^-$CD44$^+$; DN2 = CD25$^+$CD44$^+$; DN3 = CD25$^+$CD44$^-$; DN4 = CD25$^-$CD44$^-$. *WT*, wild type.

transcriptional changes were found in Notch1 targets (data not shown, supplemental Figure 5A). Furthermore, no amplification or overexpression of the p53 antagonists *Mdm2* and *Mdmx* was observed in these lymphomas (Figure 4B and supplemental Figure 5A). Western blot analysis of $Hdac1^{+/\Delta}$;$Hdac2^{\Delta/\Delta}$ and $Hdac1^{\Delta/\Delta}$ lymphomas revealed elevated p53 in combination with high p19^{Arf} expression, indicative for inactivating mutations in *p53*.[33,34] Remarkably, this was not observed in $Hdac1^{\Delta/\Delta}$;$Hdac2^{+/\Delta}$ lymphomas (Figure 5A). p53 immunohistochemical analysis of a TMA containing 50 lymphomas revealed a statistically significant decreased number of $Hdac1^{\Delta/\Delta}$;$Hdac2^{+/\Delta}$ tumors with high p53 expression compared with $Hdac1^{+/\Delta}$;$Hdac2^{\Delta/\Delta}$ and $Hdac1^{\Delta/\Delta}$ tumors ($P = .0038$; Fishers test; Figure 5B and supplemental Figure 5B). Moreover, sequencing of *p53* exons 2-11 revealed *p53* wild-type sequences in $Hdac1^{\Delta/\Delta}$;$Hdac2^{+/\Delta}$ lymphoma cell lines, while only missense mutations in the p53 DNA binding domain, a hotspot for tumor-relevant p53 mutations were found in $Hdac1^{+/\Delta}$;$Hdac2^{\Delta/\Delta}$ and $Hdac1^{\Delta/\Delta}$ lymphoma cell lines, which displayed p53 protein stabilization and p19^{Arf} expression (Figure 5C). Consistently, inhibition of Mdm2-p53 interaction using the small molecule inhibitor Nutlin-3 resulted in stabilization of p53 protein levels and cell death only in $Hdac1^{\Delta/\Delta}$;$Hdac2^{+/\Delta}$ lymphoma cell lines similar to a wild-type p53 carrying human lymphoma cell line (MOLT-3) (Figure 5D). In addition, γ-irradiation of $Hdac1^{\Delta/\Delta}$;$Hdac2^{+/\Delta}$ lymphoma cell lines resulted in increased p53 protein levels, indicative for nonmutated p53 (Figure 5E). These results indicate an Hdac1 and Hdac2 dosage dependency for inactivation of the p19^{Arf}-Mdm2-p53 tumor suppressor pathway by p53 inactivating mutations during Myc-driven lymphomagenesis.

Although $Hdac1^{\Delta/\Delta}$;$Hdac2^{+/\Delta}$ lymphomas harbor wild-type *p53* sequence, preleukemic $Hdac1^{\Delta/\Delta}$;$Hdac2^{+/\Delta}$ thymocytes showed significantly reduced p53 levels upon γ-irradiation compared with wild-type thymocytes (Figure 5F). In agreement with impaired p53 function, survival of $Hdac1^{\Delta/\Delta}$;$Hdac2^{+/\Delta}$ thymocytes was increased upon differential doses of γ-irradiation (Figure 5G). These findings suggest that reduced Hdac1- and Hdac2-governed HDAC activity in thymocytes resulted in an impaired p53 pathway, which bypasses the requirement for p53 mutations in c-Myc–induced lymphomagenesis. Consequently, impaired p53 function may allow clonal outgrowth of c-Myc overexpressing thymocytes but also tolerate mitotic slippage resulting in chromosome 15 trisomy.

Hdac1 and Hdac2 regulate Myc-collaborating genes

As transcriptional regulation is a prime function of Hdac1 and Hdac2, we used Hdac1 and Hdac2 transcriptomes in thymocytes and lymphomas to obtain insight into Hdac1/2-mediated suppression of lymphomagenesis. In agreement with reduced HDAC activity

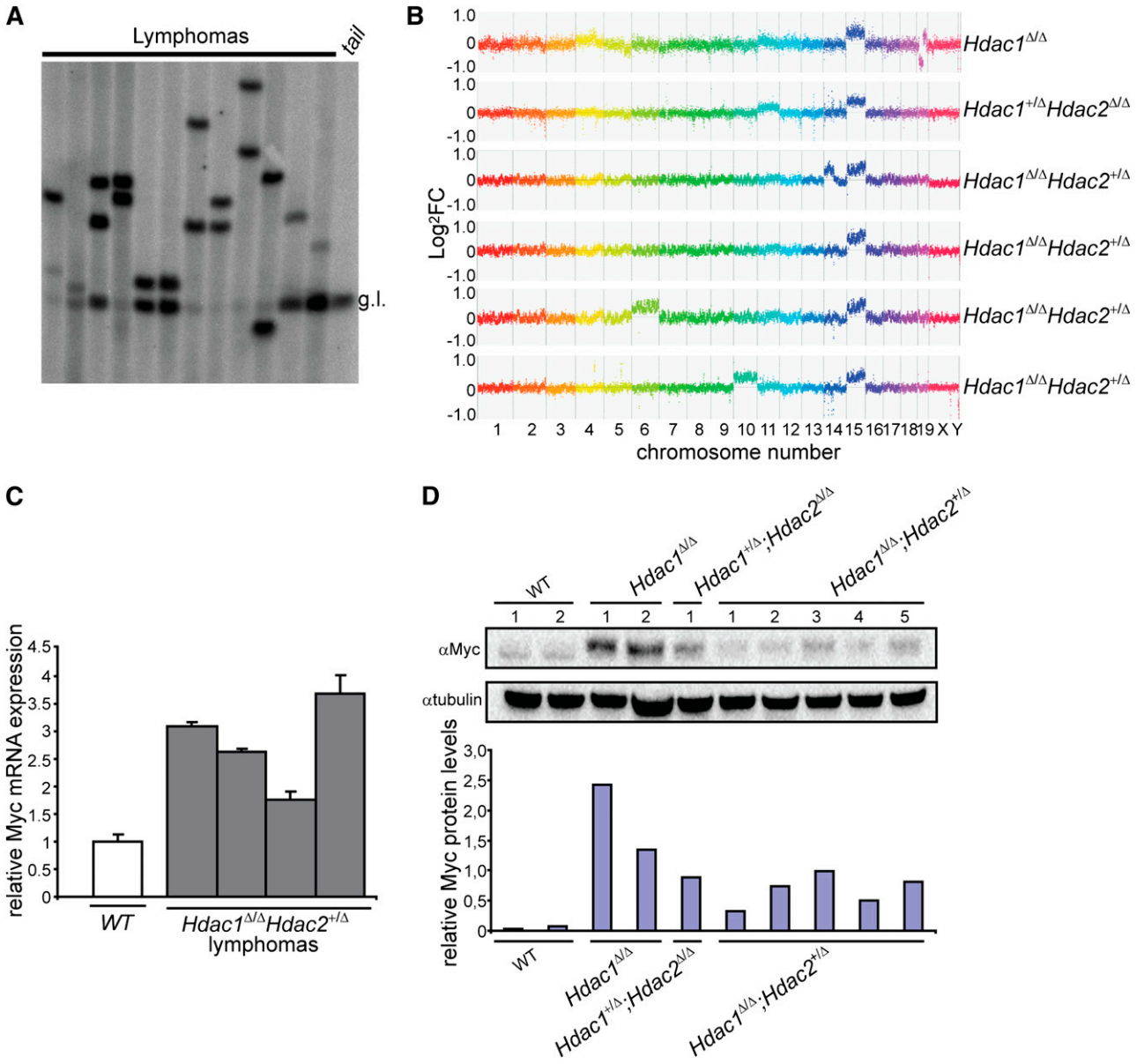

Figure 4. c-Myc overexpression–associated chromosome 15 trisomy in monoclonal T-cell lymphoma. (A) *Tcrβ* diversity in 12 independent *Hdac1*$^{\Delta/\Delta}$ *Hdac2*$^{\Delta/+}$ lymphomas analyzed by Southern blot, using a *Jβ2* region-specific probe, g.l. = germline *Tcrβ*. (B) Representative CGH plots of 6 independent lymphomas with indicated genotypes. (C) *c-Myc* levels in *WT* thymocytes and *Hdac1*$^{\Delta/\Delta}$ *Hdac2*$^{\Delta/+}$ tumors analyzed by qPCR. (D) c-Myc protein levels in wild-type thymi as well as *Hdac1*$^{\Delta/\Delta}$, *Hdac1*$^{+/\Delta}$;*Hdac2*$^{\Delta/\Delta}$ and *Hdac1*$^{\Delta/\Delta}$;*Hdac2*$^{+/\Delta}$ lymphoma cell lines. Bottom panel shows quantification of c-Myc protein levels relative to tubulin. *WT*, wild type.

(Figure 1C), *Hdac1*$^{\Delta/\Delta}$ and *Hdac1*$^{\Delta/\Delta}$;*Hdac2*$^{+/\Delta}$ thymocytes displayed increased levels of acetylated histone H4 and a dosage-dependent increase in acetylated histone ^{3}H, a hallmark of transcriptional activation (Figure 6A). Transcriptomic analysis of preleukemic thymocytes from 1- and 3- week-old *LckCre*;*Hdac1*$^{\Delta/\Delta}$;*Hdac2*$^{+/\Delta}$ mice and *Hdac1*$^{\Delta/\Delta}$;*Hdac2*$^{+/\Delta}$ tumors revealed consistent transcriptional deregulation of 547 transcripts throughout lymphomagenesis, of which 238 transcripts were also found deregulated in *Hdac1*$^{+/\Delta}$; *Hdac2*$^{\Delta/\Delta}$ and *Hdac1*$^{\Delta/\Delta}$ tumors (Figure 6B and supplemental Tables 1 and 2). In correlation with HDAC activity, tumor incidence, and tumor latency, we observed a dosage-dependent fold change in mRNA levels of many deregulated genes in *Hdac1*$^{\Delta/\Delta}$ and *Hdac1*$^{\Delta/\Delta}$; *Hdac2*$^{+/\Delta}$ thymocytes, providing a rationale for the observed dosage dependency in tumor suppression (supplemental Figure 6A and Figure 1D). Since chromosome 15 trisomy and Myc overexpression was a common feature of Hdac1/2 lymphomas, we investigated whether genes deregulated in these lymphomas were enriched for genes able to collaborate with Myc in oncogenic transformation. Among the deregulated genes we identified, a significant enrichment (164 of 410 mapped transcripts; Fisher exact test, $P = 6.^{13e\text{-}34}$) of CTGs previously found in insertional mutagenesis screens aimed at identifying Myc collaborating genes in lymphomagenesis[28,29](Figure 6C and supplemental Table 3). These data indicate that Hdac1 and Hdac2, in a dosage-dependent manner, regulate the expression of genes able to synergize with c-Myc in oncogenic transformation of thymocytes.

Expression of Jdp2 is critical for survival of Hdac1$^{\Delta/\Delta}$;Hdac2$^{+/\Delta}$ tumors

Myc collaborating genes have been shown to synergize with c-Myc by inactivating the tumor-protective p53 pathway[35] and *Hdac1*$^{\Delta/\Delta}$;

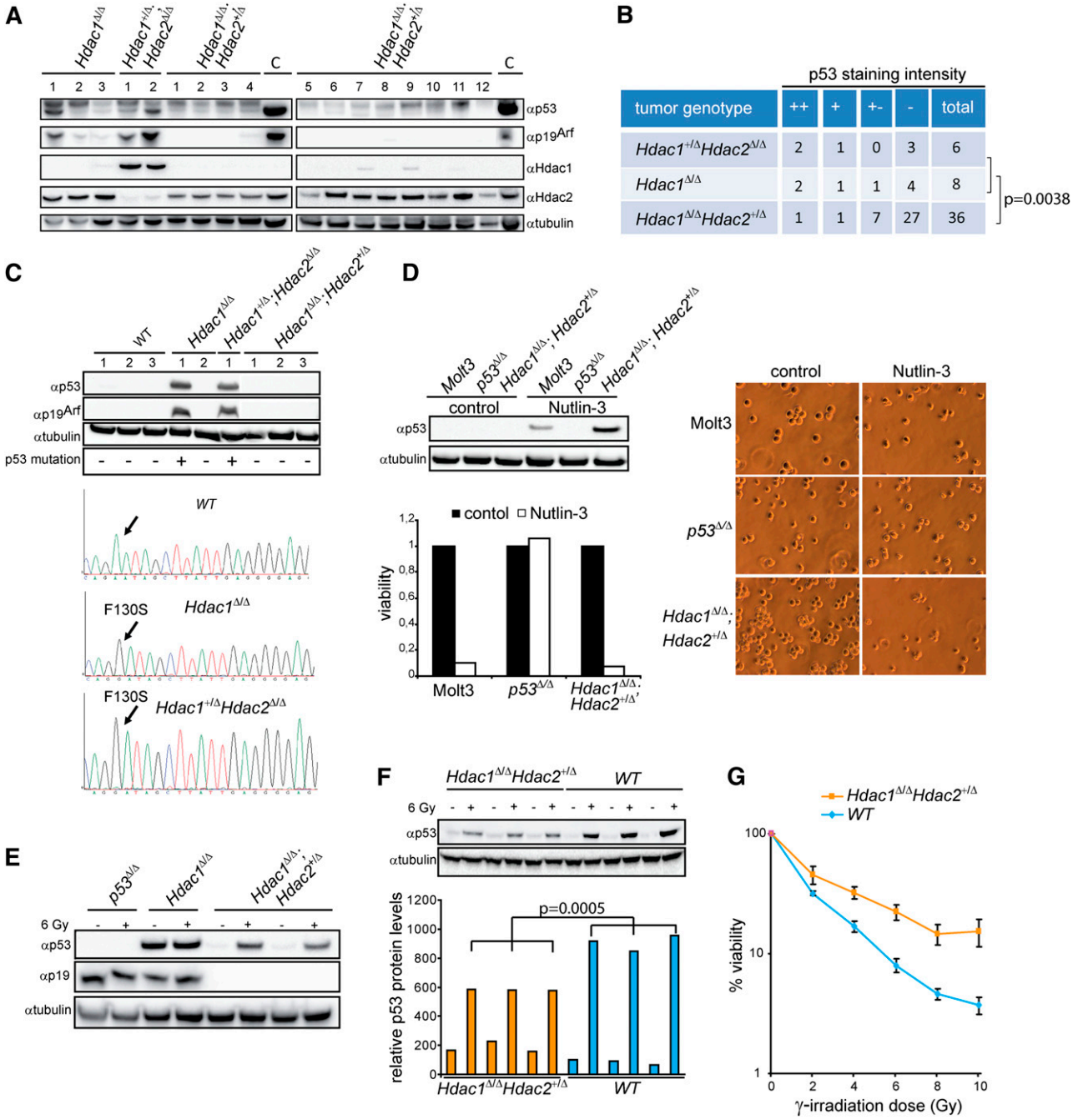

Figure 5. Hdac1 and Hdac2 dosage-dependent requirement for p53 inactivation. (A) Western blot of protein lysates from tumors with indicated genotypes using Hdac1, Hdac2, p19^{Arf}, and p53 antibodies. α-tubulin served as loading control. (B) Summary of p53 staining intensity, indicative for stabilized/mutant p53, of a tissue micro-array containing *Hdac1*$^{+/\Delta}$;*Hdac2*$^{\Delta/\Delta}$ (n = 6), *Hdac1*$^{\Delta/\Delta}$ (n = 8), and *Hdac1*$^{\Delta/\Delta}$;*Hdac2*$^{+/\Delta}$ (n = 36) tumors, revealed a significant decrease of mutant p53 in *Hdac1*$^{\Delta/\Delta}$;*Hdac2*$^{+/\Delta}$ tumors (Fisher test, $P = .0038$; bottom table). (C) Western blot analysis of *Hdac1*$^{+/\Delta}$;*Hdac2*$^{\Delta/\Delta}$, *Hdac1*$^{\Delta/\Delta}$ and *Hdac1*$^{\Delta/\Delta}$;*Hdac2*$^{+/\Delta}$ lymphoma cell lines as well as wild-type thymocytes for expression of p53 and p19^{Arf}. Tubulin served as a loading control (top). *p53* DNA binding domain missense mutations (F130S) in *Hdac1*$^{\Delta/\Delta}$ and *Hdac1*$^{+/\Delta}$;*Hdac2*$^{\Delta/\Delta}$ tumor cell lines. *p53* sequence of wild-type thymocytes served as reference (bottom). (D) Western blot analysis of Nutlin-3–treated *Hdac1*$^{\Delta/\Delta}$;*Hdac2*$^{\Delta/+}$ lymphoma cell line for expression of p53. Human MOLT-3 T-ALL cell line harboring wild-type p53 and a murine *p53*$^{\Delta/\Delta}$ T-cell lymphoma served as controls. Tubulin served as a loading control. Nutlin-3 treatment resulted only in wild-type p53 bearing lymphoma cell lines in loss of viability, as determined by cell-titer blue assay (lower panel) and visual inspection of cell cultures (right panel; magnification 200×). (E) Western blot analysis of protein lysates of *p53*$^{\Delta/\Delta}$, *Hdac1*$^{\Delta/\Delta}$, and *Hdac1*$^{\Delta/\Delta}$;*Hdac2*$^{+/\Delta}$ tumor cell lines treated with ionizing radiation (6 Gy) for p53 and p19^{Arf}. *Hdac1*$^{\Delta/\Delta}$;*Hdac2*$^{+/\Delta}$ tumor cell lines showed radiation-induced p53 in contrast to an *Hdac1*$^{\Delta/\Delta}$ lymphoma cell line expressing mutant p53. (F) Western blot analysis (top panel) of p53 protein levels in 1-week-old *WT* and *Hdac1*$^{\Delta/\Delta}$;*Hdac2*$^{\Delta/+}$ thymocytes, 6 hours after mock or 6 Gy γ-irradiation. Tubulin served as loading control. Bottom panel shows quantification of p53 levels relative to tubulin. Error bars indicate standard deviations of thymocyte cultures isolated from 3 independent mice per genotype. (G) Percentage of viable cells in 3 independent *WT* and *Hdac1*$^{\Delta/\Delta}$;*Hdac2*$^{\Delta/+}$ thymocyte cultures 24 hours after indicated doses of γ-irradiation. *WT*, wild type.

Hdac2$^{+/\Delta}$ preleukemic thymocytes display reduced p53 protein levels upon γ-irradiation. Consequently, we searched for deregulated genes in *Hdac1*$^{\Delta/\Delta}$;*Hdac2*$^{+/\Delta}$ preleukemic thymocytes known to suppress p53 function. Indeed, several Myc collaborating genes were identified that have been implicated in suppression of p53 function. These included Jun dimerization partner 2 (*Jdp2*), Juxtaposed with another zinc finger protein 1 (*Jazf1*), Dual specificity tyrosine-phosphorylation-regulated kinase 3 (*Dyrk3*), LPA receptor 2 (*Lpar2*),

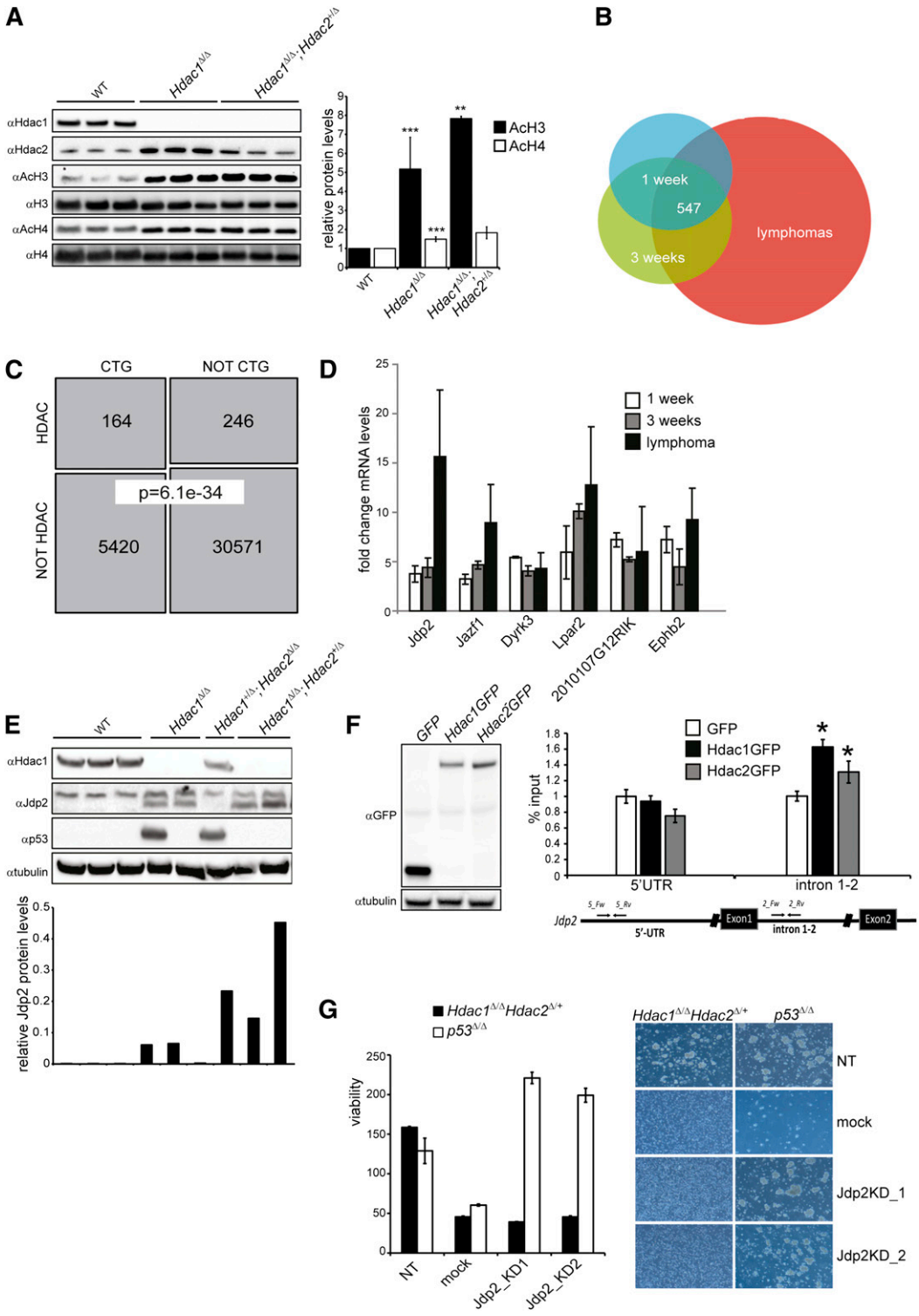

Figure 6. *Jdp2*, a Myc-collaborating gene is a direct target of Hdac1/2 and is required for the survival of *Hdac1*$^{\Delta/\Delta}$; *Hdac2*$^{+/\Delta}$ lymphomas. (A) Western blot analysis of histone H3 and H4 acetylation in nuclear lysates of preleukemic thymocytes from 3 independent 1-week-old wild-type, *LckCre*$^{+}$;*Hdac1*$^{\Delta/\Delta}$ and *LckCre*$^{+}$;*Hdac1*$^{\Delta/\Delta}$;*Hdac2*$^{+/\Delta}$ mice (left). Acetylated H3 and H4 signals were quantified over total H3 and H4 signal, respectively. While AcH3/H4 levels were significantly higher in *LckCre*$^{+}$;*Hdac1*$^{\Delta/\Delta}$;*Hdac2*$^{+/\Delta}$ and *LckCre*$^{+}$;*Hdac1*$^{\Delta/\Delta}$;*Hdac2*$^{+/\Delta}$ thymocytes compared with wild-type thymocytes, only AcH3 levels were increased in *LckCre*$^{+}$;*Hdac1*$^{\Delta/\Delta}$;*Hdac2*$^{+/\Delta}$ thymocytes compared with *LckCre*$^{+}$;*Hdac1*$^{\Delta/\Delta}$ counterparts. (B) Venn diagram demonstrating the overlap between sets of differentially expressed genes (adjusted *P* value < 0.05, fold change $\geq 1.5\times$, n ≥ 3 independent mice per group) in 1-week-old and 3-week-old *Hdac1*$^{\Delta/\Delta}$;*Hdac2*$^{\Delta/+}$ thymocytes and lymphomas. (C) Schematic representation of the overlap between CTGs identified in insertional mutagenesis screens and genes deregulated in *Hdac1*$^{\Delta/\Delta}$;*Hdac2*$^{\Delta/+}$ thymocytes and lymphomas ("HDAC"; Fisher exact test, $P = 6.36^{e-10}$). (D) Fold changes in mRNA of Myc-collaborating genes *Jdp2*, *Jazf1*, *Dyrk3*, *Lpar2*, *2010107G12RIK*, and *Ephb2* in 1-week-old and 3-week-old *Hdac1*$^{\Delta/\Delta}$;*Hdac2*$^{\Delta/+}$ thymocytes and *Hdac1*$^{\Delta/\Delta}$;*Hdac2*$^{\Delta/+}$ lymphomas, relative to age-matched wild-type thymi. (E) Western blot analysis of protein lysates of lymphomas of indicated genotypes for Hdac1, Jdp2 (lower band), and p53. Tubulin served as a loading control. (F) Western blot analysis (left) and chromatin immunoprecipitation analysis (right) of GFP, Hdac1-GFP, or Hdac2 GFP expressing *p53*$^{-/-}$ T-cell lymphoma cell lines for the Jdp2 intron 1-2 and 5′ UTR. (G) Cell viability assessed by cell titer blue assay (left) and representative images (right; magnification 100×) of *Hdac1*$^{\Delta/\Delta}$;*Hdac2*$^{\Delta/+}$ and *p53*$^{-/-}$ lymphoma cell lines infected with independent lentiviral *Jdp2* shRNA constructs (*Jdp2*_KD1 or *Jdp2*_KD2), a lentiviral nontargeting shRNA (NT) construct, or mock infection. *WT*, wild type.

a transcript with unknown function *2010107G12RIK*, and Ephrin type-B receptor 2 (*Ephb2*)[36-38] (Figure 6D). The *Jdp2* gene specifically drew our interest as *Jdp2* is targeted in insertional mutagenesis screens with high frequency in Myc overexpressing lymphomas.[28,29] In addition, *Jdp2* was preferentially activated by insertional mutagens in murine $p53^{+/-}$ lymphomas that retained the *p53* wild-type allele and was shown to suppress *p53* expression.[37] Indeed, we observed an Hdac1/2 dosage-dependent derepression of *Jdp2* in $Hdac1^{\Delta/\Delta}$ and $Hdac1^{\Delta/\Delta}$;$Hdac2^{+/\Delta}$ preleukemic thymocytes, which increased further during lymphomagenesis. Moreover, Jdp2 levels inversely correlated with the presence of stabilizing p53 mutations (supplemental Figure 6A and Figure 6D,E). These data suggest that Hdac1/2 levels directly regulate Jdp2 that subsequently, in a dosage-dependent manner, represses p53. Indeed, chromatin immunoprecipitation experiments using T-cell lymphoma cell lines expressing GFP-tagged versions of Hdac1 and Hdac2 revealed a direct binding of Hdac1 and Hdac2 to a *Jdp2* intron 1-2 promoter region in contrast to a more 5′ UTR region of the *Jdp2* locus (Figure 6F). Moreover, downregulation of *Jdp2* using 2 independent *Jdp2* shRNAs resulted in rapid cell death of $Hdac1^{\Delta/\Delta}$;$Hdac2^{+/\Delta}$ lymphoma cells but did not affect the survival of a $p53^{-/-}$ lymphoma cell line (Figure 6G and supplemental Figure 6B), suggesting that Jdp2 is critical for the survival of lymphoma cells in a p53-dependent manner. Collectively, the data presented here demonstrate that Hdac1 and Hdac2 function in a dosage-dependent manner as a p53-dependent barrier to prevent oncogenic transformation of Myc overexpressing thymocytes through transcriptional regulation of p53 suppressors like Jdp2.

Discussion

In summary, using a unique mouse model displaying a gradient of Hdac1 and Hdac2 governed HDAC activity, we provide genetic evidence for a previously unknown dosage-dependent tumor suppressor function for Hdac1 and Hdac2.

In contrast to HDAC-activity–independent chromosome 15 trisomy associated c-Myc upregulation, we observed HDAC-activity–dependent histone ^{3}H hyperacetylation and associated gene deregulation in preleukemic thymocytes. The significant enrichment of Myc-collaborating genes (MCGs) among the deregulated genes attest to the importance of Hdac1 and Hdac2 as critical regulators of genes that determine cellular fate upon oncogenic insults such as Myc overexpression. MCGs have been shown to synergize with c-Myc in tumorigenesis by inactivating the tumor-protective $p19^{Arf}$-Mdm2-p53 pathway.[35] Indeed, preleukemic thymocytes harboring relatively low HDAC activity ($Hdac1^{\Delta/\Delta}$;$Hdac2^{+/\Delta}$) displayed a dysfunctional p53 response and showed no inactivating mutations in *p53*. Consistently, several deregulated MCGs in preleukemic $Hdac1^{\Delta/\Delta}$;$Hdac2^{+/\Delta}$ thymocytes were shown to suppress p53 function. Although the pleiotropic effect caused by loss of HDAC activity suggests that multiple MCGs contributed to lymphomagenesis, Jun dimerization partner 2 (Jdp2, also known as Jundm2) seemed to play a critical role. Jdp2 was upregulated in an HDAC-activity–dependent manner in primary thymocytes as well as lymphomas and Jdp2 levels inversely correlated with p53 mutations (Figure 6E). A rationale for the latter observation is provided by the known p53 suppressing activity of Jdp2,[37] which alleviates the need to inactivate p53 upon an oncogenic insult and may also explain why activating retroviral insertions in Jdp2 strongly accelerated Myc-driven lymphomagenesis.[28,39] This explanation is further supported by observations that $p53^{+/-}$ tumors harboring *Jdp2*-activating transposon insertions retained wild-type p53.[37] Finally, ablation of Jdp2 in $Hdac1^{\Delta/\Delta}$;$Hdac2^{+/\Delta}$ lymphoma cells resulted in rapid cell death while $p53^{-/-}$ lymphoma cells remained unaffected, attesting to the p53-dependent role of Jdp2 in maintenance of tumor cells harboring wild-type p53.

We identified deregulated expression of other MCGs regulating p53 function next to Jdp2 Dyrk3 was shown to impair p53 activity through phosphorylation of Sirt1.[36] In addition, Lpar2 was shown to collaborate with c-Myc oncogenic transformation and allowed bypass of p53-induced senescence in the presence of wild-type p53, suggesting a role for Lpar2 in regulating the p53 fail-safe function.[38,40] Although we cannot exclude that these Hdac1/2–regulated genes also contributed to lymphomagenesis, the fact that these MCGs do not regulate p53 transcription suggests that Jdp2 is a crucial contributor to the tumor phenotype. Together these results indicate a role for Hdac1- and Hdac2-governed HDAC activity in preventing "transcriptional instability." Gradual loss of HDAC activity will result in a gradual increas in transcriptional instability, providing the cell with a repertoire of misexpressed proteins. Upon encountering an oncogenic insult, such as c-Myc overexpression, selection from the misexpressed protein repertoire for the most advantageous combination, including proteins inactivating p53 function, will generate a volatile situation that facilitates tumorigenesis (supplemental Figure 6C).

Previously, we showed that loss of Hdac1 and Hdac2 in mouse embryonic fibroblasts resulted in a senescence-like growth arrest independent of $p16^{Inka}$/$p19^{Arf}$ and p53, suggesting that other pathways are involved in mediating the loss of Hdac1 and Hdac2.[5] Although the mechanism underlying the developmental block during T-cell differentiation in *DKO* mice remains elusive, it is tempting to speculate that similar pathways are activated upon loss of Hdac1 and Hdac2 in thymocytes. Identification of these pathways may also provide insights into the early thymocyte block in *DKO* mice.

Our findings provide a cautionary note on the use of HDACi in the clinic as these agents may enable therapy-induced tumorigenesis. Although constitutive genetic inactivation of HDACs is different from temporal, chemical inactivation of HDAC activity using HDACi, the progression of $Hdac1^{+/\Delta}$;$Hdac2^{+/\Delta}$ thymocytes into a full-blown lymphoma suggests that prolonged subtle changes in HDAC activity may generate a tumor-prone condition that can result in lymphomagenesis. Prolonged treatment of patients with HDACi may recapitulate the partial HDAC-activity reduction as observed in *LckCre*;$Hdac1^{\Delta/\Delta}$ mice and *LckCre*;$Hdac1^{+/\Delta}$;$Hdac2^{\Delta/\Delta}$ mice. Most notably, somatic mutations in *HDAC1* were identified in 8.3% of dedifferentiated liposarcoma, providing support for a tumor-suppressive function of HDAC1 in humans.[41] Moreover, several studies have shown that inactivation of epigenetic regulators may result in adverse effects such as tumorigenesis. Genetic inactivation of the epigenetic regulators DNA methyltransferase 1 (*Dnmt1*), histone deacetylase 3 (*Hdac3*), and Sirtuin 2 (*Sirt2*) resulted in tumor formation in mouse models.[31,42,43] Moreover, cancer genome sequencing projects have revealed recurrent mutations in methyltransferase *EZH2*[44] and DNA methyl transferase *DNMT3A*,[45] underscoring the potential adverse effects of small molecule inhibitors on these enzymes in the treatment of (cancer) patients.

Although genetic alterations affecting HDAC1 and/or HDAC2 in human T-cell acute lymphoblastic lymphomas (T-ALL) have not been identified, full genome sequencing identified mutations affecting known HDAC1 and HDAC2 interactors, such as BCL11B[46] and RUNX1.[22,47] The identification of HDAC1- and HDAC2-negative tumor specimen in various other tumor types[48,49] encourages the analysis of T-cell lymphomas for HDAC1 or HDAC2 expression.

Despite the concerns raised by our studies regarding HDACi treatment, they simultaneously revealed that reduced HDAC activity

generates a cancer cell vulnerability. Since critical HDAC activity levels are required to sustain tumor cells, one can envision increased HDACi sensitivity of tumors displaying reduced HDAC activity. Less remaining HDAC activity needs to be inactivated to reach the HDAC-activity threshold that is critical for viability. Indeed, our data showed an increased responsiveness of tumors displaying relatively low HDAC activity toward pharmacological inhibition of HDACs. Therefore, identification of tumors with low HDAC levels, as has been observed in some tumor types,[48,49] in contrast to high HDAC expression, may be used as a biomarker to predict HDACi responsiveness and to stratify cancer patient populations.

Acknowledgments

The authors are grateful to Dr F. Gounari for providing the Jβ2 probe, Dr A. Aronheim for providing the Jdp2 antibody and Dr A. Peters for providing the pMR150 plasmid. The authors thank Ton Schrauwers, Corine van Langen, Auke Zwerver, Cor Spaan, and Dienke Jonkers for excellent animal care; Shan Baban and Marja Nieuwland for help with gene expression profiling; Wim Brugman for CGH analysis; Ernst-Jan Geutjes for help with cell toxicity assays; Tibor van Welsem and Fred van Leeuwen for histone H4 antibodies; Hilda de Vries for p53 reagents; and Roelof Pruntel for assistance with *p53* sequencing. The authors are grateful to Renate de Groot and Annegien Broeks for generating the tissue micro-array and to Martin van der Valk for histology review. The authors thank Drs Reuven Agami, Anton Berns, Fred van Leeuwen, and Bas van Steensel for critical reading of this manuscript and suggestions.

This work was supported by grants from the Nederlandse organisatie voor Wetenschappenlijk Onderzoek (NWO) to J.-H.D. (NWO-VIDI 864.07.008) and H.J. (NWO-VIDI 917.56.328) and the Dutch Cancer Society to J.-H.D. (KWF-2007-3978).

Authorship

Contribution: M.R.H., R.H.W., H.J., R.M.K., L.F.W., and J.-H.D. designed and planned experiments. M.R.H., R.H.W., E.Y., A.V., J.d.J., and J.-H.D. performed experiments and analyzed data. M.R.H. and J.-H.D. wrote the manuscript.

Conflict-of-interest disclosure: The authors declare no competing financial interests.

Correspondence: Jan-Hermen Dannenberg, Division of Gene Regulation, Netherlands Cancer Institute, Plesmanlaan 121, 1066 CX, Amsterdam, The Netherlands; e-mail: j.dannenberg@nki.nl.

References

1. Hanahan D, Weinberg RA. Hallmarks of cancer: the next generation. *Cell.* 2011;144(5):646-674.
2. Hagelkruys A, Sawicka A, Rennmayr M, Seiser C. The biology of HDAC in cancer: the nuclear and epigenetic components. *Handb Exp Pharmacol.* 2011;(206):13-37.
3. Yang X-J, Seto E. The Rpd3/Hda1 family of lysine deacetylases: from bacteria and yeast to mice and men. *Nat Rev Mol Cell Biol.* 2008;9(3):206-218.
4. Gregoretti IV, Lee Y-M, Goodson HV. Molecular evolution of the histone deacetylase family: functional implications of phylogenetic analysis. *J Mol Biol.* 2004;338(1):17-31.
5. Wilting RH, Yanover E, Heideman MR, et al. Overlapping functions of Hdac1 and Hdac2 in cell cycle regulation and haematopoiesis. *EMBO J.* 2010;29(15):2586-2597.
6. Haberland M, Johnson A, Mokalled MH, et al. Genetic dissection of histone deacetylase requirement in tumor cells. 2009;106(19): 7751-7755.
7. Montgomery RL, Davis CA, Potthoff MJ, et al. Histone deacetylases 1 and 2 redundantly regulate cardiac morphogenesis, growth, and contractility. *Genes Dev.* 2007;21(14):1790-1802.
8. Yamaguchi T, Cubizolles F, Zhang Y, et al. Histone deacetylases 1 and 2 act in concert to promote the G1-to-S progression. *Genes Dev.* 2010;24(5):455-469.
9. LeBoeuf M, Terrell A, Trivedi S, et al. Hdac1 and Hdac2 act redundantly to control p63 and p53 functions in epidermal progenitor cells. *Dev Cell.* 2010;19(6):807-818.
10. Ma P, Pan H, Montgomery RL, et al. Compensatory functions of histone deacetylase 1 (HDAC1) and HDAC2 regulate transcription and apoptosis during mouse oocyte development. *Proc Natl Acad Sci USA.* 2012;109(8):E481-E489.
11. Miller KM, Tjeertes JV, Coates J, et al. Human HDAC1 and HDAC2 function in the DNA-damage response to promote DNA nonhomologous end-joining. *Nat Struct Mol Biol.* 2010;17(9): 1144-1151.
12. Moresi V, Carrer M, Grueter CE, et al. Histone deacetylases 1 and 2 regulate autophagy flux and skeletal muscle homeostasis in mice. *Proc Natl Acad Sci USA.* 2012;109(5):1649-1654.
13. Lagger G, O'Carroll D, Rembold M, et al. Essential function of histone deacetylase 1 in proliferation control and CDK inhibitor repression. *EMBO J.* 2002;21(11):2672-2681.
14. Grausenburger R, Bilic I, Boucheron N, et al. Conditional deletion of histone deacetylase 1 in T cells leads to enhanced airway inflammation and increased Th2 cytokine production. *J Immunol.* 2010;185(6):3489-3497.
15. Trivedi CM, Luo Y, Yin Z, et al. Hdac2 regulates the cardiac hypertrophic response by modulating Gsk3 beta activity. *Nat Med.* 2007;13(3):324-331.
16. Zimmermann S, Zimmermann S, Zimmermann S, et al. Reduced body size and decreased intestinal tumor rates in HDAC2-mutant mice. 2007;67(19): 9047–9054.
17. Guan J-S, Haggarty SJ, Giacometti E, et al. HDAC2 negatively regulates memory formation and synaptic plasticity. *Nature.* 2009;459(7243): 55-60.
18. Minucci S, Pelicci PG. Histone deacetylase inhibitors and the promise of epigenetic (and more) treatments for cancer. *Nat Rev Cancer.* 2006;6(1):38-51.
19. Brehm A, Miska EA, McCance DJ, et al. Retinoblastoma protein recruits histone deacetylase to repress transcription. *Nature.* 1998;391(6667):597-601.
20. Luo J, Su F, Chen D, et al. Deacetylation of p53 modulates its effect on cell growth and apoptosis. *Nature.* 2000;408(6810):377-381.
21. Cismasiu VB, Adamo K, Gecewicz J, et al. BCL11B functionally associates with the NuRD complex in T lymphocytes to repress targeted promoter. *Oncogene.* 2005;24(45):6753-6764.
22. Guo H, Friedman AD. Phosphorylation of RUNX1 by cyclin-dependent kinase reduces direct interaction with HDAC1 and HDAC3. *J Biol Chem.* 2011;286(1):208-215.
23. Fischer A, Sananbenesi F, Mungenast A, et al. Targeting the correct HDAC(s) to treat cognitive disorders. *Trends Pharmacol Sci.* 2010;31(12): 605-617.
24. Christensen DP, Dahllöf M, Lundh M, et al. Histone deacetylase (HDAC) inhibition as a novel treatment for diabetes mellitus. *Mol Med.* 2011; 17(5-6):378-390.
25. Wilting RH, Dannenberg J-H. Epigenetic mechanisms in tumorigenesis, tumor cell heterogeneity and drug resistance. *Drug Resist Updat.* 2012;15(1-2):21-38.
26. Archin NM, Liberty AL, Kashuba AD, et al. Administration of vorinostat disrupts HIV-1 latency in patients on antiretroviral therapy. *Nature.* 2012; 487(7408):482-485.
27. Takahama Y, Ohishi K, Tokoro Y, et al. Functional competence of T cells in the absence of glycosylphosphatidylinositol-anchored proteins caused by T cell-specific disruption of the Pig-a gene. *Eur J Immunol.* 1998;28(7):2159-2166.
28. Uren AG, Kool J, Matentzoglu K, et al. Large-scale mutagenesis in p19(ARF)- and p53-deficient mice identifies cancer genes and their collaborative networks. *Cell.* 2008;133(4): 727-741.
29. de Jong J, de Ridder J, van der Weyden L, et al. Computational identification of insertional mutagenesis targets for cancer gene discovery. *Nucleic Acids Res.* 2011;39(15):e105.
30. Gutierrez A, Sanda T, Ma W, et al. Inactivation of LEF1 in T-cell acute lymphoblastic leukemia. *Blood.* 2010;115(14):2845-2851.
31. Gaudet F, Hodgson JG, Eden A, et al. Induction of tumors in mice by genomic hypomethylation. *Science.* 2003;300(5618):489-492.
32. Aster JC, Blacklow SC, Pear WS. Notch signalling in T-cell lymphoblastic leukaemia/lymphoma and other haematological malignancies. *J Pathol.* 2011;223(2):262-273.
33. Eischen CM, Weber JD, Roussel MF, et al. Disruption of the ARF-Mdm2-p53 tumor suppressor pathway in Myc-induced

lymphomagenesis. *Genes Dev.* 1999;13(20):2658-2669.

34. Kamijo T, Zindy F, Roussel MF, et al. Tumor suppression at the mouse INK4a locus mediated by the alternative reading frame product p19ARF. *Cell.* 1997;91(5):649-659.
35. Baxter EW, Blyth K, Cameron ER, et al. Selection for loss of p53 function in T-cell lymphomagenesis is alleviated by Moloney murine leukemia virus infection in myc transgenic mice. *J Virol.* 2001;75(20):9790-9798.
36. Guo X, Williams JG, Schug TT, et al. DYRK1A and DYRK3 promote cell survival through phosphorylation and activation of SIRT1. *J Biol Chem.* 2010;285(17):13223-13232.
37. van der Weyden L, Rust AG, McIntyre RE, et al. Jdp2 downregulates Trp53 transcription to promote leukaemogenesis in the context of Trp53 heterozygosity. *Oncogene.* 2013;32(3):397-402.
38. Kortlever RM, Brummelkamp TR, van Meeteren LA, et al. Suppression of the p53-dependent replicative senescence response by lysophosphatidic acid signaling. *Mol Cancer Res.* 2008;6(9):1452-1460.
39. Stewart M, Mackay N, Hanlon L, et al. Insertional mutagenesis reveals progression genes and checkpoints in MYC/Runx2 lymphomas. *Cancer Res.* 2007;67(11):5126-5133.
40. Taghavi P, Verhoeven E, Jacobs JJL, et al. In vitro genetic screen identifies a cooperative role for LPA signaling and c-Myc in cell transformation. *Oncogene.* 2008;27(54):6806-6816.
41. Taylor BS, DeCarolis PL, Angeles CV, et al. Frequent alterations and epigenetic silencing of differentiation pathway genes in structurally rearranged liposarcomas. *Cancer Discov.* 2011;1(7):587-597.
42. Kim H-S, Vassilopoulos A, Wang R-H, et al. SIRT2 maintains genome integrity and suppresses tumorigenesis through regulating APC/C activity. *Cancer Cell.* 2011;20(4):487-499.
43. Bhaskara S, Knutson SK, Jiang G, et al. Hdac3 is essential for the maintenance of chromatin structure and genome stability. *Cancer Cell.* 2010;18(5):436-447.
44. Nikoloski G, Langemeijer SMC, Kuiper RP, et al. Somatic mutations of the histone methyltransferase gene EZH2 in myelodysplastic syndromes. *Nat Genet.* 2010;42(8):665-667.
45. Ley TJ, Ding L, Walter MJ, et al. DNMT3A mutations in acute myeloid leukemia. *N Engl J Med.* 2010;363(25):2424-2433.
46. Gutierrez A, Kentsis A, Sanda T, et al. The BCL11B tumor suppressor is mutated across the major molecular subtypes of T-cell acute lymphoblastic leukemia. *Blood.* 2011;118(15):4169-4173.
47. Grossmann V, Kern W, Harbich S, et al. Prognostic relevance of RUNX1 mutations in T-cell acute lymphoblastic leukemia. *Haematologica.* 2011;96(12):1874-1877.
48. Weichert W, Röske A, Gekeler V, et al. Association of patterns of class I histone deacetylase expression with patient prognosis in gastric cancer: a retrospective analysis. *Lancet Oncol.* 2008;9(2):139-148.
49. Lagger S, Meunier D, Mikula M, et al. Crucial function of histone deacetylase 1 for differentiation of teratomas in mice and humans. *EMBO J.* 2010;29(23):3992-4007.